# NOTES AND CORRESPONDENCE

## A Simple Model Study of ENSO Suppression by External Periodic Forcing*

ZHENGYU LIU

*Center for Climatic Research-IES, and Department of Atmospheric and Oceanic Sciences, University of Wisconsin—Madison, Madison, Wisconsin*

4 May 2001 and 19 November 2001

ABSTRACT

The study of a forced delayed oscillator ENSO model suggests that the intensity of ENSO can be suppressed significantly by an external periodic forcing due to the nonlinear mechanism of frequency entrainment. This suppression of ENSO is most effective for ENSOs in the regime of unstable self-exciting oscillation and for forcing of frequencies close to that of ENSO. In particular, an annual cycle forcing can suppress ENSO substantially. This ENSO suppression effect by an external annual cycle is in contrast to the effect of the seasonal change of the coupled instability: the latter predominantly generates the seasonal phase locking of ENSO but has little effect on the amplitude of ENSO. Potential implications are also discussed for the evolution of ENSO in the Holocene and the observed monsoon–ENSO relationship.

### 1. Introduction

In spite of significant advances in our understanding of ENSO (e.g., McCreary and Anderson 1991; Neelin et al. 1994), the mechanism that determines the intensity of ENSO remains poorly understood. Previous studies are mostly based on a somewhat linear thinking: a more unstable mean climate state would favor a stronger ENSO. Thus, these studies have focused on the mean state and the associated instability (e.g., Fedorov and Philander 2000). Here, we will focus on a possible nonlinear mechanism that can also affect the amplitude of ENSO. This concerns an external periodic forcing, such as the annual cycle of solar insolation or monsoon wind.

Using a conceptual ENSO model, the delayed oscillator model of Battisti and Hirst (1989, hereafter BH), we show that an enhanced external periodic forcing tends to suppress ENSO through the nonlinear mechanism of frequency entrainment (Jackson 1990). The frequency entrainment refers to the mechanism by which a self-exciting oscillator will give up its independent mode of oscillation and acquire the frequency of the applied oscillating force. The concept of frequency entrainment has been applied to the study of the interaction of annual cycle and ENSO by Chang et al. (1994, 1995). The focus of this previous work, however, was on the development of chaos. The chaotic behavior of ENSO was also studied by Tziperman et al. (1994) and Jin et al. (1994) from the perspective of overlapping of nonlinear resonance with the seasonal cycle. These studies have identified two roles of the seasonal cycle on ENSO: the irregularity associated with chaotic transition and the regularity of seasonal ''phase locking.'' One issue that has not yet received much attention is the dependence of the amplitude of ENSO on the annual forcing, or more general, an external periodic forcing.

The contribution of this note is a systematic investigation of the dependence of the amplitude of ENSO on external periodic forcing. It will be shown that the main effect of an external periodic forcing is to reduce the amplitude of ENSO. Furthermore, ENSO is found to be suppressed most severely when the frequency of forcing is close to that of ENSO. Finally, some potential applications of the theory to ENSO observations, of both the past and present, are also discussed.

### 2. The effect of annual forcing

We first modify the delayed oscillator model by including an external forcing that is independent of the sea surface temperature (SST) in the eastern equatorial Pacific (see the appendix). The external wind stress can be represented as [see (A7)]

$$\tau_E^x(t) = \beta[M(t) + R(t)]. \quad (1)$$

where

* Center for Climatic Research Contribution Number 767.

*Corresponding author address:* Z. Liu, Dept. of Atmospheric and Oceanic Sciences, University of Wisconsin—Madison, 1225 W. Dayton St., Madison, WI 53706-1695.
E-mail: zliu3@facstaff.wisc.edu

$$M(t) = M_0 \sin(\omega t - \theta_M) \tag{2}$$

is an external periodic forcing and

$$R(t) = R_0 \,\mathrm{ran}(t) \tag{3}$$

is a stochastic forcing; ran($t$) is a random time series of unit standard deviation. A forcing amplitude $M_0 = 1$°C ($R_0 = 1$°C) is equivalent to an anomalous surface heat flux that generates a local SST anomaly of 1°C, or, with the standard parameter $\beta = 9.5 \times 10^{-3}$ N m$^{-2}$ °C$^{-1}$, is equivalent to an anomalous wind stress $\beta M_0 (\beta R_0)$ of about 0.01 N m$^{-2}$. [Here $M_0$ (or $R_0$) has the dimension of temperature (A7), which will usually be omitted].

With the external wind forcing, the delayed oscillator equation can be derived similar to BH [see (A8a) and (A8b)] as

$$dT/dt = \mu\{cT - cT(t-\tau) - nh^3 - b[M(t-\tau) + R(t-\tau)] + c_E(M+R)\}, \tag{4a}$$

$$h = \beta\{a_L(T + M + R) - a_W[T(t-\tau) + M(t-\tau) + R(t-\tau)]\}, \tag{4b}$$

where $T$ is the eastern Pacific SST and $h$ is the depth of the thermocline. The surface heat flux forcing is not expressed explicitly here because it can be incorporated into the wind forcing term $c_E M$ in (4a) [see (A8a)]. A nondimensional stability parameter $\mu$ is introduced such that a larger $\mu$ represents a stronger coupled instability. The case of $\mu = 1$ is the case of standard parameters of BH (see the appendix). In this case, the free linear mode is unstable such that model (4) has a self-exciting oscillation. When $\mu$ is less than 0.73, the free mode decays, and finite ENSO variability has to be sustained by stochastic climate forcing.

Our standard free ENSO ($\mu = 1$) exhibits a strong SST variability (Fig. 1a). The amplitude of ENSO, as represented by the standard deviation of monthly mean SST, $\sigma(T)$ is 3.9°C, and the average period of ENSO is 3.2 yr. As expected, ENSO events now are not phase locked with any particular calendar month (Fig. 1b).

For an annual cycle forcing, the forcing frequency in (2) adopts an annual frequency $\omega = \omega_{\mathrm{ann}}$. The phase $\theta_M$ will be specified such that the forcing peaks in July (dashed line in Figs. 2d,f), to represent, for example, the monsoon forcing. This phase prescription turns out to be unimportant for the amplitude of ENSO (not shown). Instead, the magnitude of the forcing ($M_0$) is the most important factor that determines the intensity of ENSO. Hereafter, ENSO variability will be represented by the residual SST $T_R$, which is obtained after the removal of the climatological seasonal cycle from the total SST $T$. Therefore, the amplitude of total variability and ENSO will be represented crudely by the standard deviations of total SST $\sigma(T)$ and residual SST $\sigma(T_R)$, respectively.

The impact of the annual forcing on ENSO can be seen in an example that has an annual forcing of $M_0 = 2$ imposed on the standard ENSO (Figs. 1c,d). The intensity of ENSO is weakened by 30% (cf. $T_R$ in Fig. 1c and 1a), with the amplitude reduced from $A(0) = 3.9$ to $A(2) = 2.8$. [Here $A(M_0)$ denotes ENSO amplitude $\sigma(T_R)$ under forcing of an amplitude $M_0$]. A modest annual cycle is also generated, as indicated by the difference of $T$ and $T_R$ in Fig. 1c. Interestingly, the forcing also generates an out-of-phase phase locking for ENSO, with El Niño events peaking in August but La Niña events peaking in February (Fig. 1d). This out-of-phase phase locking is in contrast to the present observations of an in-phase phase- locking, in which both the El Niño and La Niña events tend to peak in the boreal winter (Rasmusson and Carpenter 1982)—a point to be returned to later. In the mean time, the period of ENSO remains largely unchanged. When the annual forcing is further enhanced to $M_0 = 2.5$ (Figs. 1e,f), ENSO variability diminishes completely after the first few years and afterward the total SST is dominated by an annual cycle.

The suppression of ENSO is seen more clearly in a set of experiments of enhanced annual forcing (Fig. 2). For weaker forcing (about $M_0 < 1$), neither the amplitude (Fig. 2a) nor the period (Fig. 2b) of ENSO is affected substantially, although an out-of-phase phase locking is established (Fig. 2c). For a modestly strong forcing ($1 < M_0 < 2.3$), however, ENSO variability is reduced dramatically with a rapid transition from a free interannual oscillation to a forced annual cycle. The period of ENSO remains essentially unchanged (Fig. 2b). Strong annual variability emerges and eventually becomes dominant, as indicated by the difference between the total (cross) and ENSO (circle) variability in Fig. 2a. For an even stronger forcing ($M_0 > 2.3$), SST variability is dominated by an annual cycle and ENSO variability is suppressed completely (Fig. 2a).

Figure 2 illustrates the key point of the note: an enhanced annual forcing tends to change the climate variability from a free ENSO oscillation to a forced annual cycle, and therefore suppresses ENSO significantly. This change of frequency of the dominant variability from its intrinsic frequency to the forcing frequency is called frequency entrainment. Frequency entrainment is a robust phenomenon for some nonlinear oscillators, including the classic van der Pol oscillator (Jackson 1990), and was first applied to the study of climate variability by Chang et al. (1994). This phenomenon has been know at least since the time of Huygens, who observed that two clocks on the same wall (which provides the coupling mechanism) tend to keep synchronous time, provided their independent frequencies are not two far apart; Rayleigh observed a similar ''locking'' of two organ pipes or turning forks with nearly the same independent frequencies (Jackson 1990). In our case here that focuses on the one-way impact of an external forcing on ENSO, the clock analogy will be to apply an external periodic forcing on one clock. This

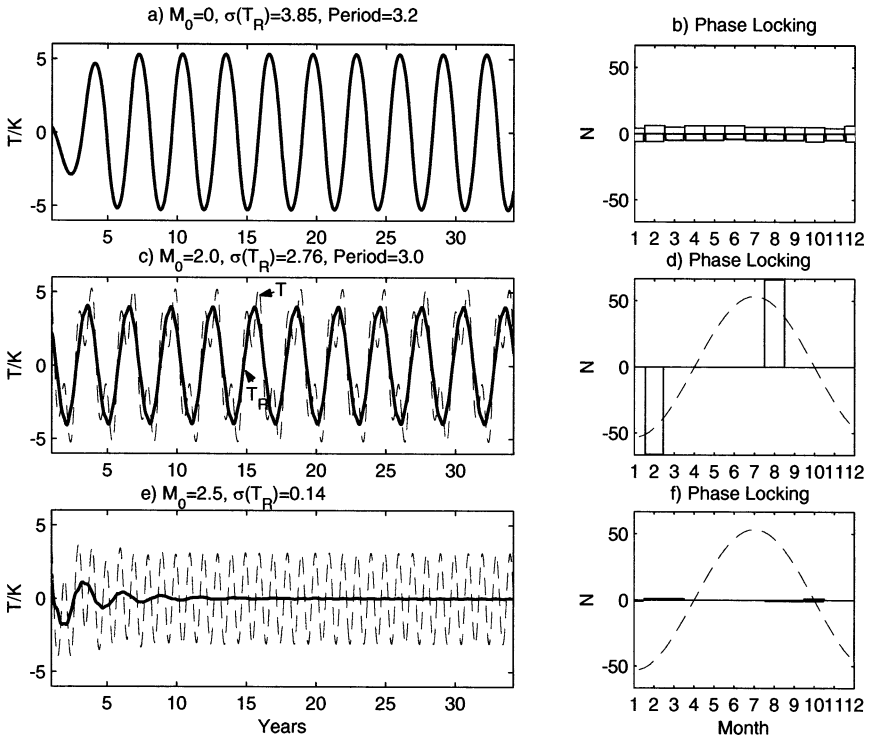


FIG. 1. Time series of total (solid, $T$) and residual (dashed, $T_R$) SSTs, and histogram of the peak months of El Niño (positive) and La Niña (negative). (a) Time series and (b) histogram for the standard self-exciting ENSO without forcing monsoon ($\mu = 1$, $M_0 = 0$, $R_0 = 0$). (c)–(d) and (e)–(f) Are the same as (a)–(b), but with a forcing of $M_0 = 2$ and $M_0 = 2.5$, respectively. The dash lines in (d) and (f) represent the annual cycle of forcing $M$ in (2) (normalized). The histograms are performed on a 200-yr time series, of which only the first 35 yr are plotted. All the time series are smoothed with a 2-month running mean and the histograms are calculated using the data after year 10. In each case, the amplitude and period of ENSO are labeled on top of the time series. The figures show a clear reduction of ENSO with the increase of the annual forcing.

forcing will make the clock lose its original frequency of oscillation and eventually, when the forcing is strong enough, oscillate with the frequency of the forcing.

In the context of the Pacific climate system, the external forcing, either wind-induced heat flux or surface heat flux, tends to force the SST to follow the annual cycle. When the forcing is strong, nonlinear response of the coupled system tends to transfer away, or dampen, the energy of intrinsic ENSO frequency, resulting in a smaller amplitude of ENSO.

Parameter sensitivity studies on the model given by (4) suggest that ENSO suppression is robust (not shown). When model parameters vary in (4a) and (4b), the forcing strength that is required for ENSO suppression increases almost linearly with the amplitude of the free ENSO $A(0)$. If we define the critical forcing strength $M_c$ as that for the $e$-folding reduction of ENSO such that $A(M_c) = A(0)/e$, the $M_c$ increases largely linearly with $A(0)$. Alternatively, if we measure the efficiency of ENSO suppression as the average sensitivity of ENSO amplitude to forcing amplitude $S_{\text{AVG}} = [A(0) - A(M_c)]/(M_c - 0)$, this efficiency does not vary substantially with model parameters. For example, nonlinearity is obviously necessary for ENSO suppression. Our studies, however, show that the efficiency of ENSO suppression remains largely unchanged for various strengths and forms of the nonlinear term in (4a). We also studied each of the four forcing terms that contributes to the external forcing [the $M$'s in (4)] and found that they all have a comparable efficiency of ENSO suppression. Therefore, the model given by (4) can be further simplified to, say, $dT/dt = -bT(t - \tau) + cT - eT^3 + c_E M$ [where $e = n(\beta a_L)^3$], while still preserving the property of ENSO suppression.

The suppression of ENSO appears to be largely insensitive to the ENSO model. We have performed a parallel study using another conceptual ENSO model—the recharge model of Jin (1997), and find that all the major conclusions of this paper remain valid there (not shown). Additional studies show that ENSO suppression also occurs in two other delayed oscillator ENSO models: the model of Suarez and Schopf (1988), (not shown) and the model of Tziperman et al. (1994) (A. Timmermann 2001, personal communication). Furthermore, ENSO suppression by seasonal forcing can also be implied from published results with intermediate coupled

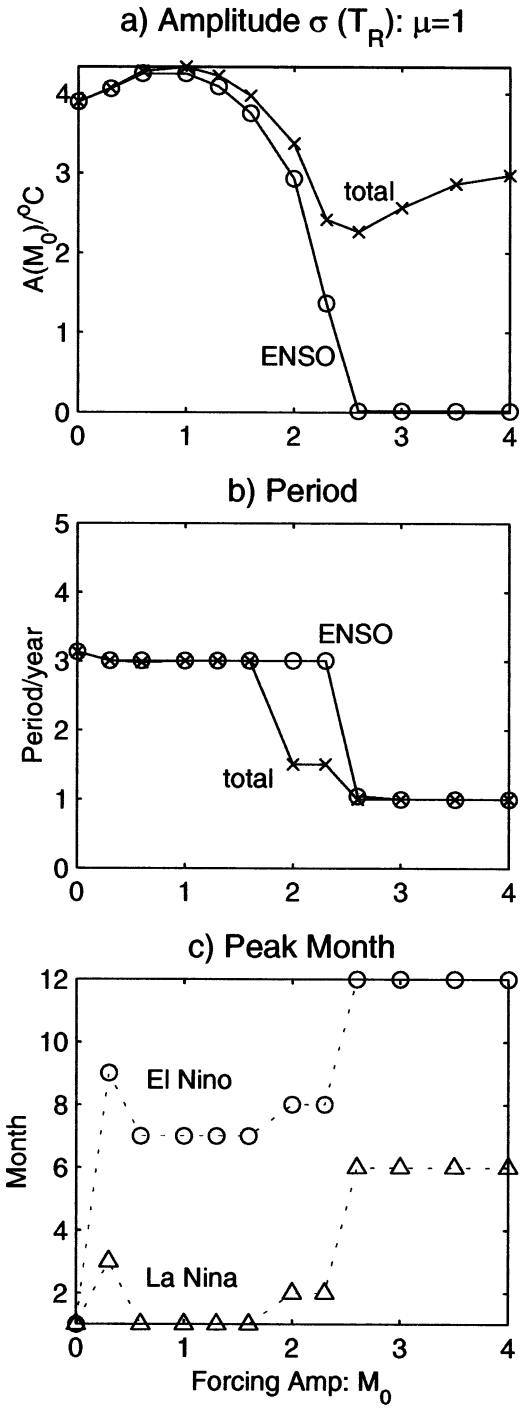


FIG. 2. Dependence of (a) amplitude and (b) average period of ENSO on forcing amplitude $M_0$ for the total (×) and residual (○) variability in the case of a self-exciting ENSO ($\mu = 1$, $R_0 = 0$). (c) The peak months for El Niño (○) and La Niña (△). The dominant variability changes from the interannual ENSO to the annual variability as a result of frequency entrainment. Here, the average period is calculated as the average intervals between two neighboring local positive peaks using the 2-month running mean SST.

ENSO models, although these studies are not designed specifically for our purpose. In the intermediate model of Chang et al. (1995), the power of interannual variability in the ENSO frequency band can be observed to decrease as the amplitude of the seasonal forcing increases (their Fig. 5). In the intermediate model of Cane and Zebiak (1985), Clement et al. (2000) recently showed that the strength of ENSO is suppressed when the amplitude of the seasonal solar insolation forcing is enhanced—a point to be returned to later.

Finally, our theory could have important application to the observed climate, because the observed climate appears to lie in a parameter regime ENSO could be affected significantly by the annual forcing. As estimated in the appendix, observations suggest that the amplitude of the present external seasonal forcing ($M$ here) ranges between about $0.35A(M)$ to $1.4A(M)$. In Fig. 2, this implies that the present ENSO is in the regime of ENSO suppression (say, $M > 1$). Otherwise, if the present climate were not deeply in the regime of ENSO suppression, we have $A(M) \approx A(0) \approx 4$, corresponding to the lower and upper bounds of $M$ as 1.4 and 5.6, respectively. This lower bound is strong enough that present ENSO could be suppressed significantly by any change of the annual forcing.

## 3. Discussions

### *a. Comparison with the effect of seasonal coupling*

We further show that ENSO suppression is caused by the part of seasonal cycle that appears as an external annual forcing on SST, rather than, for example, the seasonal change of the coupled instability associated with the seasonal change of the mean state. The latter effect has been shown responsible for the observed phase locking of ENSO (Zebiak and Cane 1987; BH; Tziperman et al. 1998).

We will replace the constant local coupled instability growth $c$ in (4a) with a seasonally varying growth rate $c_s = c[1 + s \sin(\omega_{\text{ann}} t - \theta_s)]$. As suggested by BH and Tziperman et al. (1998), the phase $\theta_s$ is such that $c_s$ peaks around July, and the amplitude of seasonality $s$ lies in the range of 0.4–0.9 for the present climate. This approach simplifies the main effect of the seasonal cycle on phase locking as the seasonal change of the coupled instability and has been used in previous studies successfully (BH; Tziperman et al. 1998). A study with the Cane–Zebiak model (Tziperman et al. 1998) has shown that the major factor that affects the seasonal change of instability, and in turn the phase locking, is the seasonal divergence field of the surface wind.

The most important effect of the seasonal coupling is the in-phase phase locking, as suggested by previous studies. This can be seen clearly in Fig. 3c for a set of experiments with enhanced seasonal coupling. In comparison, the seasonal coupling has little effect on the amplitude (Fig. 3a) and period (Fig. 3b) of ENSO within

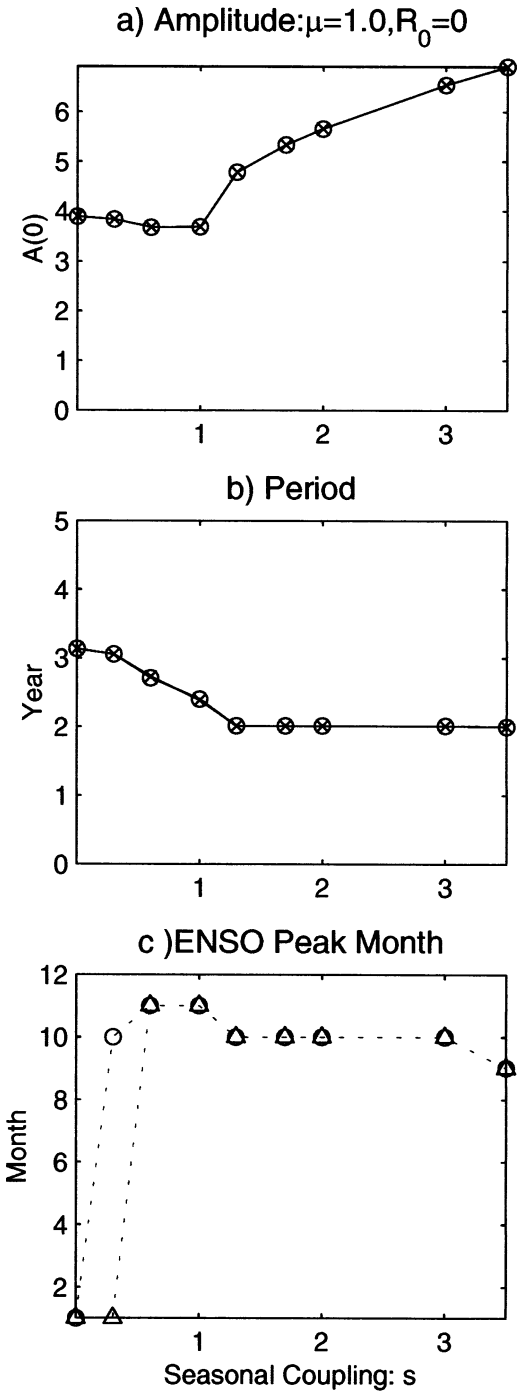


FIG. 3. Similar to Fig. 2, but as functions of the seasonal coupling $s$ for the case of the standard self-exciting ENSO ($\mu = 1$, $M_0 = 0$, $R_0 = 0$).

the realistic regime of seasonal coupling ($s < 1$). When the seasonal coupling becomes extremely strong, the SST variability is dominated by a biennial oscillation.

Major effects of the external forcing $M_0$ and the seasonal coupling $s$ can be summarized in Figs. 4a–d for the case of our standard ENSO ($\mu = 1$, $R_0 = 0$). In a broad parameter regime of realistic seasonal coupling (i.e., $0.3 < s < 1$), the amplitude of ENSO decreases with the forcing strength $M_0$, but varies little with the seasonal coupling $s$ (Fig. 4a). The weakening of ENSO with the forcing is caused by frequency entrainment as indicated by the decrease of the period of variability toward the annual period (Fig. 4b). The peak month of ENSO is determined predominantly by the seasonal coupling, such that both El Niño and La Niña tend to be locked in boreal winter (Figs. 4c,d). Mathematically, there is a clear difference between the external forcing and seasonal coupling: the former appears as an external forcing term on the right-hand side of the SST equation, while the latter appears as a variable coefficient.

### *b. Stochastically forced stable ENSO*

Stochastic forcing associated with intrinsic climate variability has recently been suggested to be important in generating ENSO variability (Penland and Sardeshmukh 1995; Moore and Kleeman 1999; Roulston and Neelin 2000). In particular, in the regime of decaying free ENSO modes [$\mu < 0.73$ in (4)], a finite ENSO has to be forced by stochastic noise. Nevertheless, all the discussions above on ENSO suppression will remain qualitatively unchanged. This can be seen by comparing the case of a stochastically forced stable ENSO ($\mu = 0.7$, $R_0 = 2$) in Figs. 4e–h with the case of the self-exciting ENSO in Figs. 4a–d. Quantitatively, however, the stochastically forced stable ENSO shows less sensitivity to the annual forcing and seasonal coupling, implying a somewhat smaller efficiency of ENSO suppression. The application of the frequency entrainment to stable ENSO, however, generalizes the original concept of frequency entrainment, which was proposed only for self-exciting (unstable) oscillators (Jackson 1990; Chang et al. 1994).

### *c. Effect of general forcing*

ENSO intensity may also be affected by other climate forcing, such as the Madden–Julian oscillation, tropical biennial oscillation, and decadal climate variability (feedbacks of ENSO on the climate forcing will not be considered here). In general, frequency entrainment could occur if the forcing frequency is close to that of the natural oscillator, as in the case of the forced van der Pol oscillator (Jackson 1990). One should therefore expect ENSO to be suppressed by external forcing of periods longer or shorter than ENSO. This is confirmed by examining the response of ENSO to a more general periodic forcing $M$ in (2) with different frequencies. Figures 5a,b shows the response of the standard self-exciting ENSO ($\mu = 1$, $R_0 = 0$) to the forcing of different periods. The amplitude of ENSO (Fig. 5a) and total (Fig. 5b) variability are plotted for 4 forcing amplitudes: $M_0 = 0$ (free ENSO, ○), 1 (+), 2 (□), and 3 (◇). Analogous to the case of annual forcing, the am-

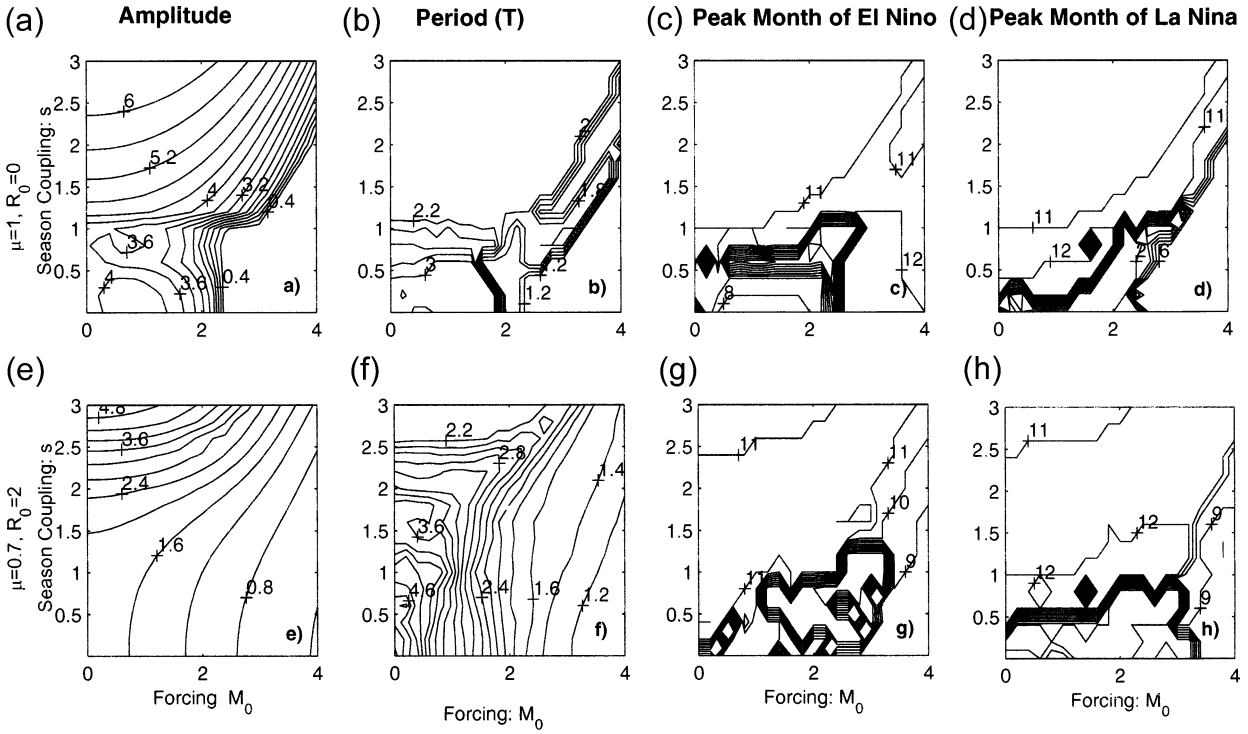


FIG. 4. (a) Amplitude, (b) period, (c) peak months for El Niño, and (d) La Niña as functions of the amplitude of annual forcing $M_0$ and seasonal coupling $s$ in the case of a self-exciting ENSO without stochastic forcing ($\mu = 1$, $R_0 = 0$). (e)–(h) Same as (a)–(d), except for a stochastically forced stable ENSO ($\mu = 0.7$, $R_0 = 2$). Contour intervals are 0.4 for the amplitude, 0.2 for the period, and 1 for the peak months.

plitude of ENSO is now calculated using the residual SST in which the composite ''climatological cycle'' of SST variability of the forcing frequency is subtracted. Figure 5a shows clearly that ENSO is suppressed at all the frequencies, if the forcing is strong enough. For a given forcing frequency, ENSO usually weakens and the total variability strengthens with an enhanced forcing. This is similar to the case of the annual forcing discussed before. Given a forcing magnitude, however, ENSO is suppressed most severely when the forcing frequency is close to that of ENSO (about 3.2 yr in this case). A high-frequency forcing at a semiannual or even annual period suppresses ENSO effectively only for very strong forcing. At biennial to decadal periods, however, ENSO is suppressed dramatically even with very weak forcing. This may imply a sensitive interaction between ENSO and, say, the tropical biennial oscillation (TBO). In addition, when the forcing period increases toward decadal, the suppression of ENSO amplitude appears to become somewhat weaker. Finally, all the major features of ENSO suppression remain qualitatively unchanged in the case of a stochastically forced stable ENSO ($\mu = 0.7$, $R_0 = 2$; Figs. 5c,d), although the efficiency of ENSO suppression is somewhat reduced.

Finally, it is interesting to consider how the amplitude of ENSO varies with enhanced stochastic forcing. A truly random forcing has a white spectrum. The intensity of ENSO therefore depends on the competition of the enhancement effect due to the linear resonance to forcing components of frequencies of ENSO, and the suppression effect due to nonlinear frequency entrainment by forcing components of frequencies different from ENSO. Figure 6 shows two examples of ENSO response to stochastic forcing. For a self-exciting ENSO ($\mu = 1$), the amplitude of ENSO decreases with an intensified random forcing (Fig. 6a). For a stochastically forced stable ENSO ($\mu = 0.7$), however, the amplitude of ENSO first increases with the stochastic forcing (till $R_0 = 4$) due to linear resonance, and then decreases due to nonlinear frequency entrainment (Fig. 6b). Therefore, ENSO suppression due to frequency entrainment tends to be dominant for a self-exciting ENSO, but it becomes important for stochastically forced stable ENSO only when the forcing is very strong. This is reasonable because a self-exciting ENSO has a stronger nonlinearity and in turn frequency entrainment.

## 4. Summary and implications

This study calls for more intensive studies on the mechanism that affects the amplitude of ENSO. Here, a conceptual ENSO model is used to study the effect of an external periodic forcing on the amplitude of ENSO. It is found that nonlinear frequency entrainment enables an external forcing to suppress ENSO signifi-

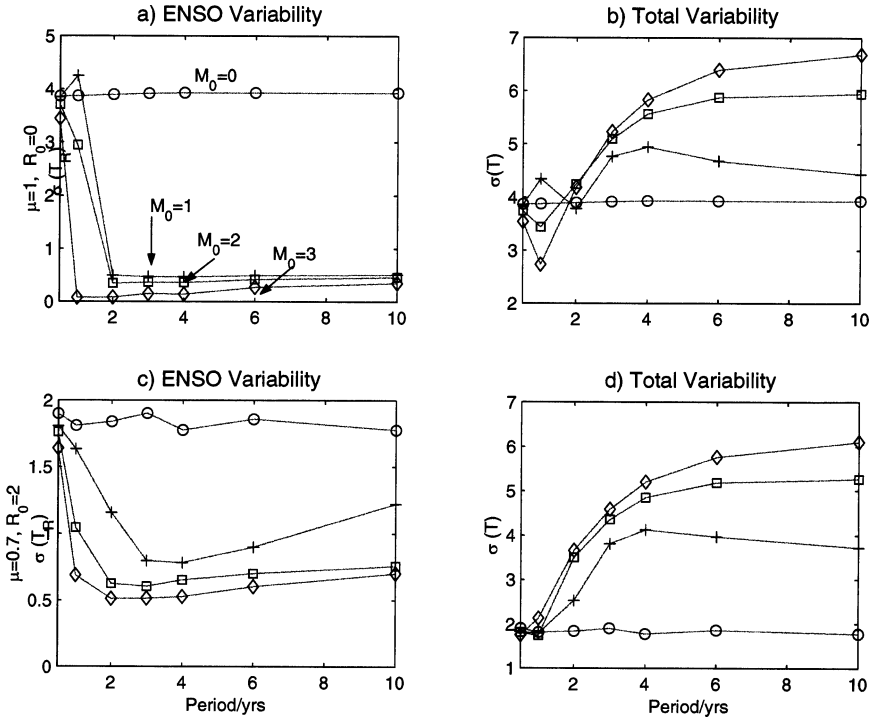


FIG. 5. The amplitude of (a) ENSO and (b) total variability as a function of the period of the forcing for the case of a self-exciting ENSO ($\mu = 1$, $R_0 = 0$). Four forcing amplitudes are used: $M_0 = 0$ (circle), 1 (plus), 2 (square), and 3 (diamond). (c)–(d) Same as (a)–(b), except for the case of a stochastically forced stable ENSO ($\mu = 0.7$, $R_0 = 2$).

cantly. In contrast to an external annual forcing, the seasonal variation of the coupled instability tends to generate the observed phase locking of ENSO events, but has little effect on the amplitude of ENSO. Furthermore, ENSO is suppressed most severely by the forcing that has a frequency close to that of ENSO. ENSO suppression is robust for model ENSOs in different stability regimes and the suppression occurs regardless of stochastic forcing. The efficiency of ENSO suppression, however, is reduced for more stable ENSOs. Thus, our contribution is the highlight of external periodic forcing as a potential mechanism that affects the amplitude of ENSO.

The effect of external periodic forcing, such as an annual forcing, on ENSO suppression seems to be more general and robust than its effect on the development of ENSO chaos. First, even in a weakly nonlinear van der Pol oscillator that has no chaos, one can show analytically that frequency entrainment occurs (Jackson 1990). Second, we have seen that even for stable ENSO

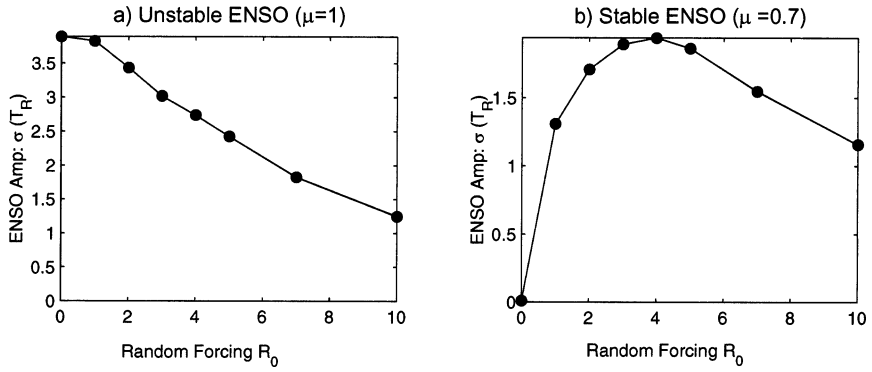


FIG. 6. ENSO amplitude as a function of the amplitude of the random forcing $R_0$ for (a) a self-exciting ENSO ($\mu = 1$, $M_0 = 0$) and (b) a stable ENSO ($\mu = 0.7$, $M_0 = 0$). The amplitude of ENSO $\sigma(T_R)$ is now the same as that of the total variability $\sigma(T)$ because of the absence of a basic climatological cycle.

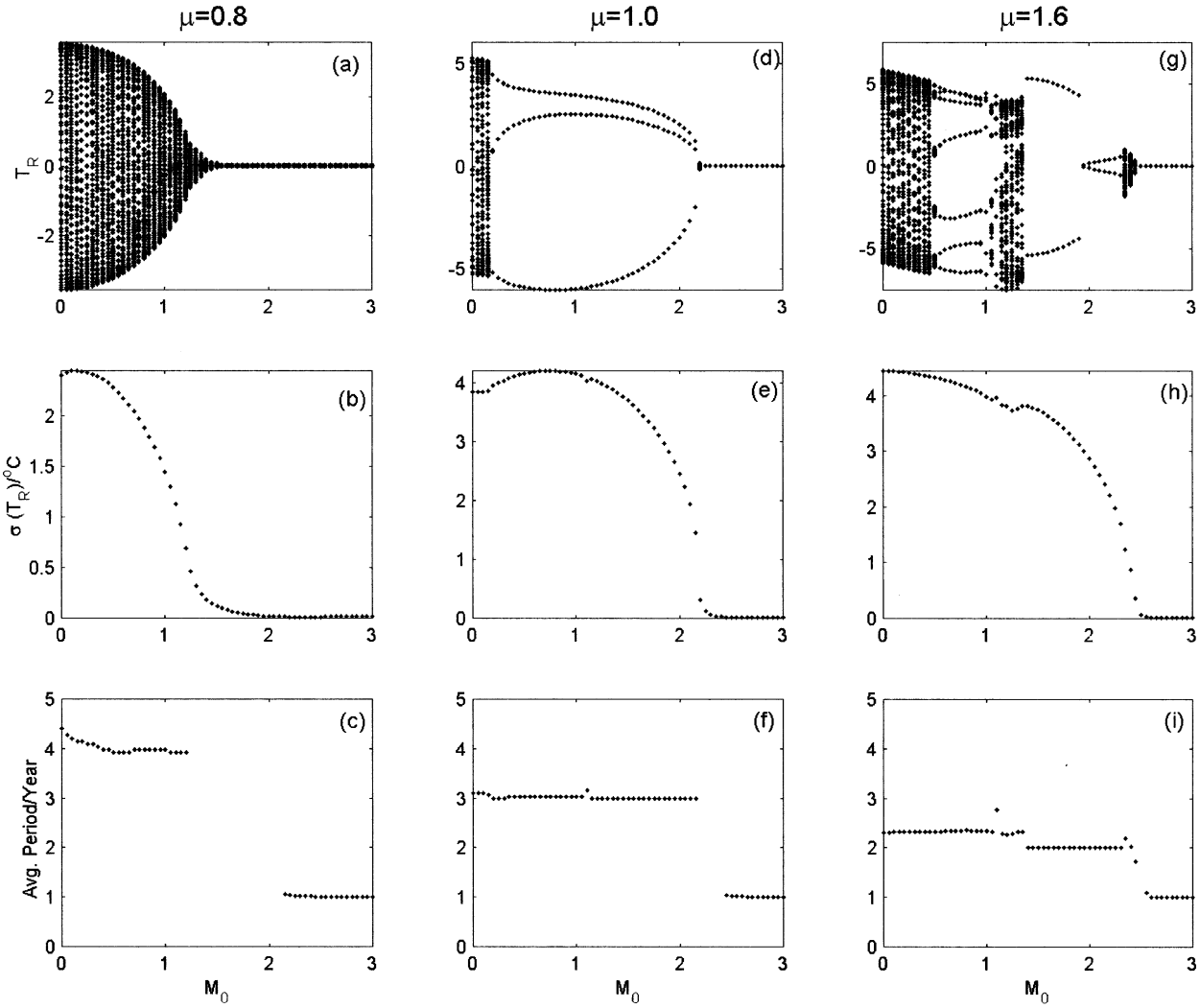


FIG. 7. The recurrence map of (top) SST, (middle) ENSO amplitude, and (bottom) average period for three sets of experiments. For the set of weakly nonlinear ENSO ($\mu = 0.8$) in (a), the anomalous SST of each 1 Jan is plotted for each $M_0$ annual forcing. The amplitude and average period in (b) and (c) are calculated similar to those in Figs. 2a and 2b for the residual SST $T_R$. Each experiment is integrated for 200 yr, of which the last 170 yr are used for the plot. (d)–(f) Same as (a)–(c) but for the standard nonlinearity of $\mu = 1$, and (g)–(i) same as (a)–(c) but for a stronger nonlinearity of $\mu = 1.6$. The recurrence map can identify the regime of frequency locking (Arnol'd tongues), in which the period of ENSO is a rational multiple of the annual period and therefore only a finite number of SSTs are repeatedly plotted for each $M_0$. The non-frequency-locking regimes in the recurrence map consist of two subregimes: quasiperiodic (period is an irrational multiple of the annual period) and chaotic oscillation, both of which will have SST values filling an entire section of SST axis (if the time series are long enough). Our further detailed calculation (not shown) shows that in the non-frequency-locking regimes in Figs. 7a, 7d, and 7g, only the regime of $1 < M_0 < 1.3$ in Fig. 7g is chaotic.

(that has no low-order chaos), ENSO suppression by external forcing is robust (Figs. 4e–h; Figs. 5c,d; Fig. 6b). Therefore, ENSO suppression occurs regardless of the chaotic nature of ENSO. This point can be further seen for unstable ENSOs in Fig. 7, which shows three sets of experiments. In each set, the amplitude of ENSO is suppressed as the forcing amplitude increases (Figs. 7b,e,h) and the average period is changed only slightly before the variability is completely entrained by the annual cycle under strong annual forcing (Figs. 7c,f,i). The suppression of ENSO are therefore similar to all other cases discussed previously. In contrast, the nonlinear oscillation behavior of ENSO varies significantly among the three sets, or even in each set for different experiments. This can be seen in the 1-yr lag SST recurrence maps (Figs. 7a,d,g). For the weak nonlinear case ($\mu = 0.8$; Fig. 7a), no frequency locking (Arnol'd tongue) exists and all ENSOs are quasiperiodic (with period of an irrational multiple of the annual period). For the standard ENSO ($\mu = 1$; Fig. 7d), ENSOs are dominated by a frequency-locking to a 3-yr cycle, as indicated clearly by a broad Arnol'd tongue ($0.2 < M_0 < 2.2$). For the strong nonlinear case ($\mu = 1.6$; Fig. 7g), ENSO exhibits a quasiperiodic oscillation for $M_0 < 0.5$; it is frequency

locked in an Arnol'd tongue for $0.5 < M_0 < 1$; it exhibits quasiperiodic and chaotic behavior for $1 < M_0 < 1.3$; it is frequency locked again in Arnol'd tongues for $1.3 < M_0 < 2.3$, and exhibits quasiperiodic oscillation for $2.3 < M_0 < 2.4$ before finally it is completely entrained into the annual cycle for $M_0 > 2.4$. Despite the complex transition of oscillation behavior with the enhanced annual forcing, the amplitude of ENSO simply decreases smoothly in all the cases. It therefore appears that there is no clear connection of the oscillation behavior of ENSO to its amplitude suppression. Instead, the amplitude suppression is more robust and exhibits simpler and more uniform behavior across the ENSO regime; it occurs in weakly nonlinear cases without chaos or strongly nonlinear cases with chaos. The robustness of ENSO suppression is important for practical reasons: we may not be able to tell if the observed ENSO is in a chaotic or stochastic regime, but ENSO suppression is always effective.

Several examples of the potential applications of this work are discussed below. Our work here was originally motivated by an attempt to understand the evolution of ENSO in the Holocene. Paleoproxy records suggest that ENSO did not become active until the mid-Holocene (about 6000 years ago; Rodbell et al. 1999). The mechanism for the reduced ENSO activity before mid-Holocene seems to be controversy. Based on a coupled GCM study, Liu et al. (2000) proposed a remote effect due to the enhanced summer monsoon wind from Asia and North America; based on an intermediate coupled model study, Clement et al. (2000) proposed a local mechanism due to the enhanced summer insolation on the equatorial Pacific. These two seemingly different mechanisms can be unified in terms of frequency entrainment. Indeed, both mechanisms resort to an enhanced annual cycle forcing: Liu et al. for the wind [$M$ in (A8)], while Clement et al. for the heat flux [$Q$ in (A8)]. In both cases, the timing of the forcing, relative to the peak timing of El Niño, is considered to be critical. The forced delayed oscillator model study suggests that the amplitude of ENSO is rather insensitive to the timing of the annual forcing (not shown). Assuming this true in the GCM or the intermediate coupled model, both previously proposed mechanisms are then incorrect, partially. Instead, it is best to attribute the two mechanisms of ENSO suppression to a common and more fundamental mechanism: the nonlinear frequency entrainment.

The nonlinear entrainment may also explain some aspects of present ENSO variability. One application is the observed interdecadal modulation of Asian monsoon strength and ENSO intensity. Observations show that ENSO is usually weak in the decades of anomalously strong Asia monsoon, and vise versa (Krishnamurthy and Goswami 2000). For example, the 20-yr running mean of all Indian rainfall correlates negatively with the standard deviation of the Niño-3 SST in successive, sliding 20-yr sections at $-0.65$ (J. Fasullo 2001, personal communication). Our study here may offer an explanation to this decadal modulation of ENSO. In the decades of stronger Asian monsoon, the intensified summer Asia monsoon enhances the summer trade wind, and in turn the seasonal cycle of the trade wind anomaly, in the equatorial Pacific (Barnett et al. 1989), which then leads to the suppression of ENSO through frequency entrainment. This decadal modulation of ENSO can be simulated in our model by prescribing an interdecadal modulation of the annual forcing (not shown).

Our study may also have implications to the observed negative correlation of the interannual variability of the Indian monsoon rainfall in summer and the El Niño event in the following winter (Shukla 1987; Webster et al. 1998). First, we notice in Figs. 1c and 1e that frequency entrainment enables an annual forcing, such as the monsoon, to suppress ENSO at a timescale shorter than that of ENSO. This rapid ENSO suppression suggests that an anomalously strong (weak) monsoon in summer could be followed by an anomalously weak (strong) El Niño in the following winter. This speculation is confirmed in our model given by (4). Forced by a random modulation (a random noise filtered by an 1-yr running mean) of the annual cycle wind $M$, the resulted SST shows a negative maximum correlation with the monsoon precipitation (using $-M$ as a proxy) when the monsoon rainfall leads El Niño by about half a year (not shown). This negative correlation of interannual variability of monsoon and ENSO could therefore be associated with ENSO suppression due to frequency entrainment. The lagged response of ENSO to monsoon may reflect an active role of monsoon in forcing ENSO. Hence, even though the origin of ENSO is independent of monsoon (Cane and Zebiak 1985), the amplitude of ENSO could be modulated by the monsoon.

Our results may imply a strong interaction of ENSO with the TBO of the Asian monsoon system. The TBO has a quasi-2-yr period (e.g., Lau and Shen 1988; Meehl 1997; Li et al. 2001), which is very close to the intrinsic period of ENSO. Since frequency entrainment is the most effective when the forcing frequency is close to the oscillation frequency (Fig. 5), the TBO should be more effective to affect the amplitude of ENSO than the annual forcing. The opposite is also true: ENSO could be very effective to affect the amplitude of TBO. Therefore, the TBO and ENSO may be closely interacting with each other, generating substantial modulation of the amplitude of each other.

These applications are speculative in nature. Our study here is extremely idealized and much further work is needed to quantify the effect of frequency entrainment on ENSO in a more realistic setting. In particular, it is desirable to systematically investigate the role of frequency entrainment on the amplitude of ENSO in an intermediate coupled model, such as the model of Zebiak and Cane (1987) or Chang et al. (1994). Furthermore, it should also be recognized that ENSO can feed back on other climate variability, such as the annual

cycle (Gu and Philander 1995). Therefore, it is important to study the feedback of ENSO on other climate variability modes, and, eventually, the interaction between ENSO and other climate variability modes.

*Acknowledgments.* I would like to thank Dr. J. Fasullo for observational plots related to the decadal modulation of Asian monsoon on ENSO, Dr. A. Timmerman for a stimulating discussion on the chaotic nature of ENSO, Ms. Y. Zhong for the calculation of the GISST, and Dr. S. Vavrus for comments on an earlier version of the paper. Comments from two reviewers have helped to improve the paper substantially. This work is supported by NSF and NOAA.

## APPENDIX

### The Model

The external heat flux and wind stress forcing can be incorporated into the delayed oscillator model of BH. (The reader should refer to BH for more details and notations). Linearized on the annual mean state,[1] the perturbation SST equation is (Zebiak and Cane 1987):

$$\frac{\partial T}{\partial t} = -\overline{\mathbf{u}}\cdot\nabla T - \mathbf{u}\cdot\nabla\overline{T} - \delta\Delta(\overline{w})\frac{\partial T}{\partial z} - \delta H(\overline{w})w\frac{\partial \overline{T}}{\partial z} - a_s T + Q. \quad \text{(A1)}$$

Here, $Q = R/c_p\rho H$ and $R$ is the surface heat flux. In the eastern equatorial Pacific, the vertical temperature gradient is given by

$$\partial_z T = (T - T_s)/H_1, \quad \text{(A2)}$$

where the subsurface temperature depends on the anomalous thermocline depth $h$ as

$$T_s = a(\overline{h})h - e^*h^3, \quad \text{(A3)}$$

with $a$ and $e^*$ being positive coefficients. The thermocline anomaly is driven by both the local and remote wind forcing, and the effect of the remote wind reaches the eastern Pacific thermocline with a delay time of $\tau$, that is,

$$h = h_{\text{Local}} + h_{\text{Remote}},$$
$$h_{\text{Local}} = -a_L\langle\tau^x\rangle, \quad h_{\text{Remote}} = -a_W\langle\tau^x(t-\tau)\rangle, \quad \text{(A4)}$$

where $\langle\ \rangle$ denotes the average over the eastern equatorial Pacific. The anomalous upwelling depends on the wind stress as

$$w = -\gamma\langle\tau^x\rangle. \quad \text{(A5)}$$

With an external wind $\tau_E^x$ that is independent of the eastern Pacific SST, the total wind stress anomaly can be represented as

$$\tau^x = \beta\langle T\rangle + \tau_E^x, \quad \text{(A6)}$$

where $\beta$ is a coupling coefficient. The external wind has a deterministic part $\beta M$ and a stochastic part $\beta R$ as

$$\tau^x = \beta(\langle T\rangle + M + R). \quad \text{(A7)}$$

Using (A2)–(A7) and averaging (A1) in the eastern equatorial Pacific lead to the delayed oscillator equation in the presence of external forcing as

$$dT/dt = cT - bT(t-\tau) - nh^3 + c_E(M+R) - b[M(t-\tau) + R(t-\tau)] + \langle Q\rangle, \quad \text{(A8a)}$$

where the thermocline anomaly is

$$h = \beta\{a_L(T + M + R) - a_W[T(t-\tau) + M(t-\tau) + R(t-\tau)]\}. \quad \text{(A8b)}$$

The parameters, following BH, are $b = K\beta\, a_W$, $c_E = K\beta\, a_L + K_E\beta\,\gamma$, $c = c_E + K_A - \hat{K} - a_s$, and $n = \hat{K}e^*$ (refer to BH for the definitions of $K$, $K_A$, $K_E$, and $\hat{K}$). Typical parameter values are set the same as the standard case in BH: $K = 2.7 \times 10^{-8}$ °C m$^{-1}$ s$^{-1}$, $K_E = 2.5 \times 10^{-2}$ °C m$^{-1}$, $\hat{K} = 1.8 \times 10^{-7}$ s$^{-1}$, $K_A = 7.3 \times 10^{-8}$ s$^{-1}$, $a_L = 750$ m$^3$ N$^{-1}$, $a_W = 370$ m$^3$ N$^{-1}$, $a_s = 9.1 \times 10^{-8}$ s$^{-1}$, $\tau = 180$ days, $\beta = 9.5 \times 10^{-3}$ N m$^{-2}$ °C$^{-1}$, $\gamma = 3.3 \times 10^{-4}$ m$^3$ N$^{-1}$ s$^{-1}$, $e^* = 3 \times 10^{-5}$ °C m$^{-2}$.

In general, it is difficult to estimate the present climate state in the context of our simple model (A8a) and (A8b). In the case of the seasonal forcing, nevertheless, crude upper and lower bounds could be found for the amplitude of the external annual forcing. The idea is to derive the upper bound from the total annual cycle of observed SST and the lower bound from the annual SST variability forced by the solar radiation alone. We should first notice (see section 2) that in our idealized model the important information for ENSO suppression is the relative strength of the external forcing (combined effect of $M$ and $Q$, denoted as, say, $F$) and ENSO. Standard deviations of SST variability are derived from the Global sea Ice and Sea Surface Temperature (GISST) data (1900–93) for the total annual variability ($F_{\text{total}}$) and interannual ENSO variability [$A(F)$] along the equatorial (5°S–5°N) Pacific, using the SST anomalies of the climatological annual cycle and in the 1.5–7-yr band, respectively. [Similar results are obtained using the Comprehensive Ocean–Atmosphere Data Set (COADS; da Silva et al. 1994)]. Averaged in the central-eastern Pacific (east of 180°), the total annual variability and ENSO variability have the amplitude of $F_{\text{total}} \approx 1$°C and $A(F) \approx 0.7$°C, respectively, or $F_{\text{total}} \approx 1.4\, A(F)$. Since the total annual cycle includes the external annual cycle forcing ($F$), which is independent of the eastern Pacific SST, as well as the internal

[1] The annual cycle in the mean state is not considered here, because we focus on the external annual cycle forcing, which turns out to have effects very different from those due to the annual cycle in the mean state (see section 3a). When studying the phase locking in section 3a, the annual cycle of the mean state is approximated by the annual change of the coupled instability, as in previous simple model studies (e.g., Tziperman et al. 1998).

annual cycle variability, which depends on ocean–atmosphere feedback in the eastern Pacific (Mitchell and Wallace 1992; Liu and Xie 1994; Chang and Philander, 1994), $F_{\text{total}}$ only provides an upper bound for $F$. To estimate the external forcing $F$ would require knowledge of the relative magnitude of the external and internal annual cycle.

Alternatively, we derived a lower bound by only considering the part of equatorial annual SST variability forced by the heat flux forcing $Q$ alone (neglecting the wind-forced part). The annual cycle of the shortwave radiation forcing $R_S$ (from Berger 1978) in the equatorial band (5°S–5°N) is used to drive a slab mixed layer SST according to $c_p\rho H_m\, dT/dt = R_S - \lambda T$. Here, $H_m = 50$ m is the mixed layer depth and $\lambda = 30$ W m$^{-2}$ K (Haney 1971) is a climate sensitivity. A large negative feedback damping $\lambda$ is used here because we want to exclude the part of SST amplification due to positive tropical ocean–atmosphere feedbacks. The resulting SST variability, which is dominated by an annual cycle, has a standard deviation of $0.25°\text{C} = 0.35\, A(F)$. Therefore, the external annual forcing $F$ lies in the range of $0.35\, A(F)$ to $1.4\, A(F)$.

## REFERENCES


Barnett, T. P., L. Dumenil, U. Schlese, E. Roeckner, and M. Latif, 1989: The effect of Eurasian snow cover on regional and global climate variations. *J. Atmos. Sci.,* **46,** 661–685.

Battisti, D. S., and A. C. Hirst, 1989: Interannual variability in a tropical atmosphere–ocean model: Influence of the basic state, ocean geometry, and nonlinearity. *J. Atmos. Sci.*, **46,** 1687–1708.

Berger, A. L., 1978: Long-term variations of daily insolation and quaternary climatic changes. *J. Atmos. Sci.,* **35,** 2362–2367.

Cane, M. A., and S. E. Zebiak, 1985: A theory for El Niño and the Southern Oscillation. *Science,* **228,** 1084–1087.

Chang, P., and G. Philander, 1994: A coupled ocean–atmosphere instability of relevance to the seasonal cycle. *J. Atmos. Sci.,* **51,** 3628–3648.

——, B. Wang, T. Li, and L. Ji, 1994: Interactions between the seasonal cycle and the Southern Oscillation—frequency entrainment and chaos in a coupled ocean–atmosphere model. *Geophys. Res. Lett.,* **21,** 2817–2820.

——, L. Ji, B. Wang, and T. Li, 1995: Interactions between the seasonal cycle and El Niño–Southern Oscillation in an intermediate coupled ocean–atmosphere model. *J. Atmos. Sci.,* **52,** 2353–2372.

Clement, A. C., R. Seager, and M. A. Cane, 2000: Suppression of El Niño during the mid-Holocene by changes in the Earth's orbit. *Paleoceanography,* **15,** 731–741.

da Silva, A. M., C. C. Young, and S. Levitus, 1994: *Anomalies of Directly Observed Quantities.* Vol. 2, *Atlas of Surface Marine Data 1994,* NOAA Atlas NESDIS 7, 416 pp.

Fedorov, A., and G. Philander, 2000: Is El Niño changing? *Science,* **288,** 1997–2002.

Gu, D., and S. G. H. Philander, 1995: Secular changes of annual and interannual variability in the Tropics during the past century. *J. Climate,* **8,** 864–876.

Haney, R. L., 1971: Surface thermal boundary condition for ocean circulation models. *J. Phys. Oceanogr.,* **1,** 241–248.

Jackson, E. A., 1990: *Perspectives of Nonlinear Dynamics.* Vol. 1, Cambridge University Press, 496 pp.

Jin, F.-F., 1997: An equatorial ocean recharge paradigm for ENSO. Part I: Conceptual model. *J. Atmos. Sci.,* **54,** 811–847.

——, D. Neelin, and M. Ghil, 1994: El Niño on the Devil's staircase: Annual subharmonic steps to chaos. *Science,* **264,** 70–72.

Krishnamurthy, V., and B. N. Goswami, 2000: Indian Monsoon–ENSO relationship on interdecadal timescales. *J. Climate,* **13,** 579–595.

Lau, K.-H., and P. J. Shen, 1988: Annual cycle, quasi-biennial oscillation, and Southern Oscillation in global precipitation. *J. Geophys. Res.,* **93,** 10 945–10 988.

Li, T., C.-W. Thaw, and C.-P. Chang, 2001: A coupled air–sea–monsoon oscillator for the tropospheric biennial oscillation. *J. Climate,* **14,** 752–764.

Liu, Z., and S. P. Xie, 1994: Equatorward propagation of coupled air–sea disturbances with application to the annual cycle of the eastern tropical Pacific. *J. Atmos. Sci.,* **51,** 3807–3822.

——, J. Kutzbach, and L. Wu, 2000: Modeling climatic shift of El Niño variability in the Holocene. *Geophys. Res. Lett.,* **27,** 2265–2268.

McCreary, J. P., and D. Anderson, 1991: An overview of coupled ocean–atmosphere models of El Niño and the Southern Oscillation. *J. Geophys. Res.,* **96,** 3125–3150.

Meehl, G. A., 1997: The south Asian monsoon and the tropospheric biennial oscillation (TBO). *J. Climate,* **10,** 1921–1943.

Mitchell, T., and M. Wallace, 1992: On the annual cycle in equatorial convection and sea surface temperature. *J. Climate,* **5,** 1140–1156.

Moore, A. M., and R. Kleeman, 1999: Stochastic forcing of ENSO by the intraseasonal oscillation. *J. Climate,* **12,** 1199–1220.

Neelin, J. D., M. Latif, and F.-F. Jin, 1994: Dynamics of coupled ocean–atmosphere models: The tropical problem. *Annu. Rev. Fluid Mech.,* **26,** 617–659.

Parker, D. E., P. D. Jones, C. K. Folland, and A. Bevan, 1994: Interdecadal changes of surface temperature since the late nineteenth century. *J. Geophys. Res.,* **99,** 14 373–14 399.

Penland, C., and P. Sardeshmukh, 1995: The optimal growth of the tropical sea surface temperature anomalies. *J. Climate,* **8,** 1999–2024.

Rasmusson, E. M., and T. H. Carpenter, 1982: Variations in tropical sea surface temperature and surface wind fields associated with the Southern Oscillation. *Mon. Wea. Rev.,* **110,** 354–384.

Rodbell, D. T., G. O. Seltzer, D. M. Anderson, M. B. Enfield, D. B. Newman, and H. Jeremy, 1999: An ~15 000-year record of El Niño—Driven alluviation in southwestern Ecuador. *Science,* **283,** 516–520.

Roulston, M. S., and J. D. Neelin, 2000: The response of an ENSO model to climate noise, weather noise, and intraseasonal forcing. *Geophys. Res. Lett.,* **27,** 3723–3726.

Shukla, J., 1987: Interannual variability of monsoons. *Monsoons,* J. S. Fein and P. L. Stephens, Eds., John Wiley and Sons, 399–464.

Suarez, M. J., and P. S. Schopf, 1988: A delayed action oscillator for ENSO. *J. Atmos. Sci.,* **45,** 549–566.

Tziperman, E., L. Stone, M. Cane, and H. Jarosh, 1994: El Niño chaos: Overlapping of resonances between the seasonal cycle and the Pacific Ocean–atmosphere oscillator. *Science,* **264,** 72–74.

——, M. A. Cane, and S. E. Zebiak, 1995: Irregularity and locking to the seasonal cycle in an ENSO-prediction model as explained by the quasiperiodicity route to chaos. *J. Atmos. Sci.,* **52,** 293–306.

——, ——, ——, Y. Xue, and B. Blumenthal, 1998: Locking of El Niño's peak time to the end of the calendar year in the delayed oscillator picture of ENSO. *J. Atmos. Sci.,* **55,** 2191–2199.

Webster, P. J., V. O. Magana, T. N. Palmer, J. Shukla, R. A. Tomas, M. Yanai, and T. Yasunari, 1998: Monsoons: Processes, predictability, and the prospects for prediction. *J. Geophys. Res.,* **103** (C7), 14 451–14 510.

White, W. B., 1995: Design of a global observing system for gyre-scale upper ocean temperature variability. *Progress in Oceanography,* Vol. 36, Pergamon, 169–217.

Zebiak, S. E., and M. A. Cane, 1987: A model El Niño–Southern Oscillation. *Mon. Wea. Rev.,* **115,** 2262–2278.